A comprehensive study of Q-factor using synthetic trace modeling and real data analysis from Búzios oil field

Gustavo Souza[1], Leonardo Miquelutti[1], Paulo H. B. Alves[1], Henrique B. Santos[1], Marco Cetale[1], [1]UFF/PPGDOT/GISIS

Abstract

In this work, we conducted a comprehensive analysis to determine the Q-factor in synthetic data using three frequency-domain techniques: spectral ratio, peak frequency shift, and centroid frequency shift methods. Our experiments involved the generation of attenuated seismic traces, followed by an exploration of various approaches to accurately recover the true Q-factor attenuation applied to these traces. Leveraging prior knowledge of reflection events, we focused on optimizing the recovery process. Furthermore, we applied these techniques to estimate the Q-factor along a seismic line in the Búzios oil field, in the Santos Basin, Brazil, relying on geological interpretation of the relevant horizons. Our findings shed light on the efficacy of these methods for Q-factor estimation and provide valuable insights into the Q-factor characteristics within the Santos Basin.

Introduction

Seismic wave propagation in real media differs from ideal elastic solids due to effects such as attenuation and dispersion. Attenuation refers to the decrease in wave amplitude with distance, while dispersion causes different spectral components to travel at different speeds, distorting the waveform. These phenomena are influenced by elastic and inelastic processes, where energy is preserved or converted into heat. Seismic absorption is related to frequency, with higher frequencies experiencing more absorption.

In exploration, understanding inelastic attenuation is important as it relates to porous spaces and fluid-filled rock pores. Petrophysical properties can be inferred through seismic interpretation, and absorption provides valuable additional information.

Inelastic attenuation can be quantified by the attenuation coefficient and a dimensionless quantity known as the Quality factor (Q factor). According to Kolsky (1964); Kjartansson (1979); Wang (2008), the attenuation coefficient represents the individual energy loss for each frequency and exhibits linear behavior with the angular frequency and the tangent of phase delay (or loss angle) $\tan(\delta)$ as indicated by Equation 1.1:

$$\alpha = \frac{\omega \tan \delta}{2v(\omega)} \tag{1}$$

where $v(\omega)$ is the phase velocity of the P-wave.

Inelastic attenuation, commonly referred to as attenuation, has an inversely proportional relationship with the Q factor. The Q factor can be expressed as the ratio between the total energy of the wavefront E_0 in one cycle and the change in energy ΔE in the subsequent cycle Knopoff and MacDonald (1958):

$$Q = \frac{2\pi E_0}{\Delta E} \tag{2}$$

The relationship between the Q factor and the attenuation coefficient can be expressed by the following equations:

$$Q = \frac{\omega}{2\alpha v(\omega)} \tag{3}$$

$$\alpha = \frac{\omega \tan \delta}{2v(\omega)} = \frac{\omega}{2v(\omega)Q} = \frac{\pi}{\lambda Q} \tag{4}$$

where λ represents the wavelength of the seismic wave.

Therefore, the present study aims to understand the effects of attenuation and its estimation in different scenarios. We conducted several experiments varying parameters of trace generation and attenuation, and varying estimation techniques using three methods. After validating the methodology, the estimation functions were applied to real seismic data from the Santos Basin.

Attenuation theory

We generated the attenuated synthetic traces used for evaluating the estimation methodologies of the Q factor using two distinct mechanisms: the Simple Exponential Attenuation (5) and the Kolsky attenuation mechanism (8).

Exponential simple decay mechanism

This method assumes an exponential decay of the frequency spectrum described by Equation 5 below:

$$Y(f,t) = Y(f) \cdot \exp\left(-\frac{\pi f t}{Q}\right) \tag{5}$$

Equation 5 allows for calculating a spectrum $Y(f,t)$ at any time t and frequency range f based on a reference spectrum $Y(f)$.

Kolsky Mechanism

The Kolsky attenuation 1956 is a more robust mechanism widely used in seismic trace filtering due to its applicability (Wang, 2008). This mechanism is based on the propagation of one-way unidirectional waves to generate seismic pulses in the time domain. The governing equation for this method is presented as follows:

$$U(r+\triangle r,\omega)=U(r,\omega)\exp((\frac{\omega}{\omega h})^{-\gamma}\frac{\omega\triangle T}{2Qr})\exp(i(\frac{\omega}{\omega h})^{-\gamma}\omega\triangle T), \tag{6}$$

where $U(r+\triangle r,\omega)$ represents a pulse that has traveled a distance $\triangle r$ for all frequencies ω, $U(r,\omega)$ represents the wavefield in the with angular frequency , r is the distance of the pulse from the origin, i is the imaginary unit where Qr is a reference Q factor in the medium, vr is the reference phase velocity, and h is the highest angular frequency present in the amplitude spectrum of the trace, i.e., the Nyquist frequency.

The first exponential term is responsible for the attenuation, while the second term is responsible for the dispersion of the propagated pulse. Considering that $U(T,\omega)$ is a pulse in time T for all frequencies , the image condition determining the pulse amplitude only in the time domain is given by the following integration:

$$U(T+\triangle T,\omega)=\frac{1}{\pi}\int_0^\infty U(T+\triangle T,\omega)d\omega, \tag{7}$$

where $U(T+\triangle T)$ is the pulse amplitude in the time domain at time $T+\triangle T$, and $U(T+\triangle T,\omega)$ is the filtered spectrum at time $T+\triangle T$ for all frequencies . In practice, the trace in the time domain $U(T)$ is filtered from the complete spectrum of a generic trace, where the pulse amplitudes are identical. Then, a pre-filtered trace is conditioned solely by performing the Fourier transform, collecting the amplitudes of the positive.

Q estimation theory

Now we describe the 3 methods employed in this work for estimating the Q-factor of an attenuated seismic signal: Spectral ratio method (SRM), Centroid frequency shift method (CFSM), and Peak frequency shift method (PSFM).

Spectral ratio method (SRM)

The spectral ratio method is based on the assumption that the decay of energy in spectra can be approximated by an exponential function. Therefore, for a constant Q factor, a given time instant t_2 greater than t_1, and a frequency range f, it is possible to estimate the Q factor by filtering and analyzing the spectra using the following relationship:

$$A(f)=\frac{ln(Y(f,t_2)}{ln(Y(f,t_1)}=\frac{\pi(t_2-t_1)f}{Q}\therefore Q=\frac{\pi(t_2-t_1)}{p}, \tag{8}$$

where $Y(f,t2)$ represents a new spectrum with reduced amplitude due to energy loss at high frequencies. Taking the natural logarithm of the spectral ratio results in a linear trend. Let $A(f)$ be a function dependent on frequency f, and let p be the slope coefficient formed by the linear portion of the $A(f)f$ line. In this study, the method of linear least squares is employed to obtain the slope coefficient of the logarithm of the spectral ratio.

Centroid frequency shift method (CFSM)

The frequency centroid shift method was introduced by Quan and Harris (1997) with the aim of generating an initial estimate in VSP data and performing well-to-well attenuation tomography. The frequency centroid f_c is defined based on a given amplitude spectrum, representing the frequency that contains half of the energy of the spectrum. Essentially, the signal spectrum $S(f)$ is integrated in relation to the amplitude spectrum, with f_c being the geometric center of the amplitude spectrum $S(f)$.

$$f_c=\frac{\int_0^\infty f\dot{S}(f)df}{\int_0^\infty S(f)df} \tag{9}$$

The variance $\sigma^2 S$ of the spectrum $S(f)$ is calculated as follows.

$$\sigma_S^2=\frac{\int_0^\infty (f-f_c)^2 S(f)df}{\int_0^\infty S(f)df} \tag{10}$$

Thus, the frequency centroid is obtained using a formula for calculating the geometric center of an arbitrary function.

$$Q=\frac{\pi t\sigma_0^2}{f_{c0}-f_{c1}} \tag{11}$$

This method determines the Q factor based on the movement of the frequency centroid towards lower frequencies over time. To accomplish this it is required a reference spectrum that closely matches the frequency signature of the seismic source used in data acquisition.

Peak frequency shift method (PFSM)

The peak frequency shift method, initially described in the work of Zhang and Ulrych (2002), estimates the Q factor in seismic records organized in families of common midpoints. The main objective is to measure the shift of the peak energy in the amplitude spectrum with respect to the pulse propagation time. The works of Gamar-Sadat et al. (2015) and Ramos et al. (2019) use a variation of the mentioned method to generate initial models utilized in the Q-factor tomography and compensate for absorption in real data. Therefore, starting from a reference peak frequency f_m, we can estimate the Q factor using a peak frequency of a propagated pulse f_p:

$$Q=\frac{\pi f\triangle t f_p f_m^2}{2(f_m^2-f_p^2)}, \tag{12}$$

where Δt is the time difference between the compared pulses and f represents the frequencies present in the spectrum.

In the absence of knowledge about the reference peak frequency, Zhang and Ulrych (2002) present an alternative method to calculate it using the amplitude of a reflection hyperbola in a common midpoint seismic record as follows:

$$f_m = \sqrt{\frac{f_{p1} f_{p2} (t_2 f_{p1} - t_1 f_{p2})}{t_2 f_{p2} - t_1 f_{p1}}} \tag{13}$$

The variables f_{p1} and f_{p2} correspond to the peak frequencies of pulses at times t_1 and t_2, respectively, in the same reflection hyperbola in a common midpoint seismic record.

Methodology

To validate the employed techniques, we generated a trace with no dispersion/attenuation by convolving a Ricker wavelet with a reflectivity profile, and then we attenuated it accordingly to the two previously mentioned mechanisms (simple decay and Kolsky's mechanism) and four different Q-factor values (50, 75, 150 and 200). The reflectivity profile was comprised of reflection events of equal intervals, amplitude, and Q-factor among themselves. The wavelet, reflectivity profile, and generated traces for $Q = 150$ are shown in Figure 1. Throughout the experiments, we varied both the parameters for generating the synthetic trace and/or the parameters for estimating the Q-factor.

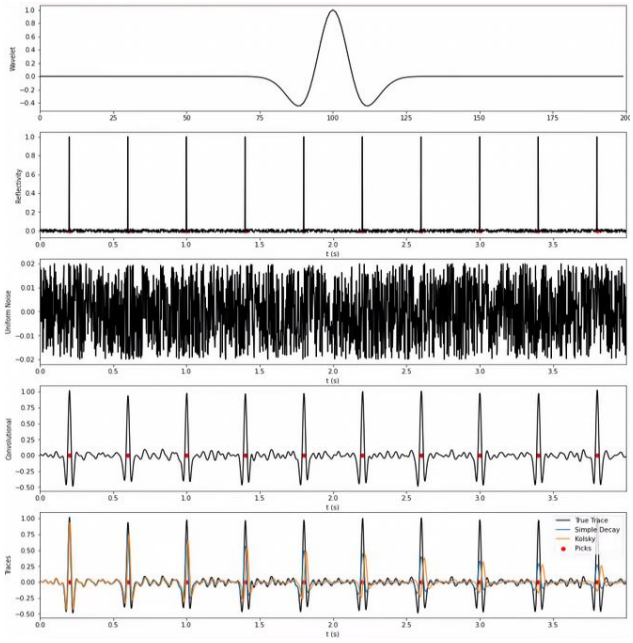

Figure 1: The upper panel shows the wavelet used for the convolution with the reflectivity profile in the second panel. The third displays a random noise of 0.02. The fourth shows the trace prior to the attenuation process, while the fifth panel displays the attenuated noisy traces (either through simple decay and Kolsky's mechanism). The red dots indicate the *time* of the reflection events.

We performed several experiments varying some aspects in the trace generation with a Q-constant factor, and/or in the Q-factor estimation, as:

- reference spectrum
- spectral interpolation
- frequency range considered
- addition of noise
- data smoothing
- data windowing
- length of the pulse
- weighted least squares

We compared the results through both a qualitative analysis of the pulse spectrum, as well as quantitatively by comparing the estimated Q values with the original Q value of each trace. After we analyzed the effects of varying such parameters in the Q-factor estimation in synthetic data, we then applied it in a real seismic survey line from Santos Basin.

Important to highlight a point here: throughout the whole set of experiments with synthetic data, we provided the *time* of the reflection events as input. Therefore, we also provided that for real data application, and we retrieved such information from the seismic interpretation of the main horizons of interest.

In all experiments with synthetic data, we did the following:

1. Extracted each pulse with an (input) *window length* $winlen$ from the seismic trace according to the (input) *time* (the $picktime$ variable) each occurred.
2. Performed some operation on each pulse (time domain) - *optional*.
3. Calculated the spectrum of each pulse.
4. Performed some operation on each pulse's spectrum (frequency domain) - *optional*.
5. Defined/input the *reference spectrum*, i.e. the spectrum at the time t_1 in Equations (8), (10), and (13).
6. Used the methods SRM, CFSM, and PFSM to calculate the Q-factor of the seismic trace between each pair of events using the chosen *reference spectrum*.

In all experiments, the $picktime$ (red dots in Figure 1) was defined as the time of the events in the reflectivity profile used to generate the synthetic signal. Also, we used $2ms$ as the *sample time* Δt for the trace generation.

The experiments are described below. Each item line describes a new experiment:

1. We chose $winlen = 0.1s$, and did nothing in the pulses in both time and frequency domain (steps 2 and 4 in the workflow previously mentioned). We also set that this pulse with length $= 0.1s$ would be completed with 0's to match 2000 samples (we called this variable $fillvalue$).
2. We tested varying the *reference spectrum* allowing it to be the spectrum of a Ricker's wavelet, of the first pulse, or of the previous pulse (to the pulse of interest).

3. We interpolated the pulse spectrum (step 4 in the workflow), as it affects how it locates the peak and centroid frequencies.
4. We used only half of the frequency range previously used for the SRM. The frequency cutoff went from $5Hz$ to $35Hz$.
5. We added noise to the generated signal, adding it to the reflectivity profile prior to the convolution. From this experiment on, we only used noisy synthetic traces.
6. We smoothed the extracted pulses (step 2 in the workflow).
7. We tested the effect of different tapers in the extracted pulses, as Hanning window, or DPSS, from Slepian (1978).
8. We change the $winlen$ and the $picktime$.
9. We tested the effect of the variable $fillvalue$ as it affects the spectrum resolution. Bigger $fillvalue$ yields more frequencies to evaluate the spectrum at than short ones.
10. We compared the *weighted least squares* weighted by the spectrum amplitude to regular least squares.

Then, for real-data application, we selected a seismic line from the Santos basin and, departing from the interpretation of its seismic section:

1. we retrieved the time of the events of interest (the $picktime$ in the synthetic experiments).
2. Hence, we associated seven reflection events to each trace of the seismic section, comprising the ocean bottom, post-salt, the salt itself, and pre-salt horizons (reflection events).
3. Then, we varied some of the parameters described in the experiments with synthetic data,
4. and plotted the Q-factor corresponding section.

We describe the results in the next section.

Results

We now describe the results with both synthetic and real data.

Study with synthetic data

We experimented with a whole set of parameters variation, and conclude the following:

- The PSFM and CFSM are sensible to spectrum resolution in the sense of frequency content; i.e. smaller $fillvalue$, which in turn yielded a smaller number of frequencies, resulted in less variations in the peak/centroid frequency due to the lower number of frequencies yielded by the Fourier transform.
- The SRM improved when we halved the frequency content for the calculation. This happens because the higher frequencies showed higher variations than lower ones in the log of spectral ratio.
- Among all procedures we performed on the pulses in the time domain, its tapering with 0^{th}-order DPSS ($NW = 3$) was the one that better improved the results, yielding Q-factor estimated values much closer to real one when we added noise to the signal.
- The SRM performed better when the *reference spectrum* was chosen as the previous pulse to the pulse representing the reflection event of interest, while both the CFSM and FPSM performed better with the Ricker wavelet as reference.
- The weighted least squares did not improve the results over regular least squares.

Figure 2 shows the results for the three methods in the first experiment (without noise in the trace). The upper panel shows the attenuated traces, while the three others show the results for SRM, PFSM, and CFSM. Even after we added noise, we greatly improved our results with the use of DPSS, as we can see in Figure , which shows this and other experiments' results with the synthetic trace attenuated by the Kolsky mechanism. We chose to show only the results retrieved from traces attenuated with the Kolsky mechanism because they imposed a bigger challenge in the Q-factor estimation than simple decay attenuated traces.

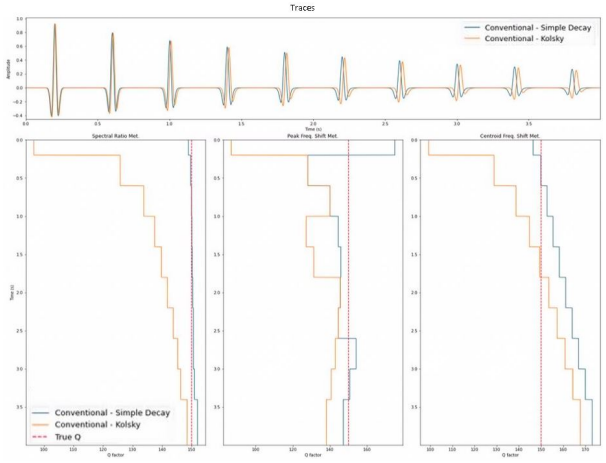

Figure 2: Q-factor estimations from noiseless data for both attenuation mechanisms.

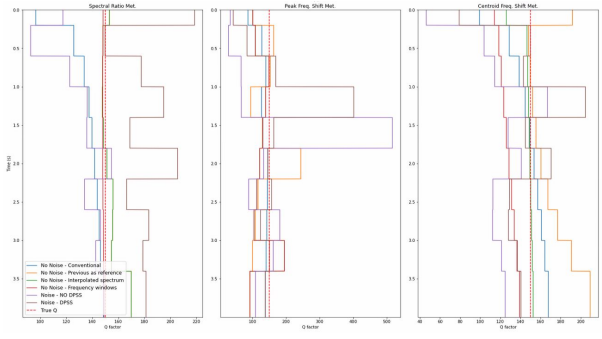

Figure 3: Q-factor estimations for several experiments.

The spectra of the pulses retrieved from the trace used to obtain Figure are shown in Figure 4. Figure 4-a and -b

show the spectra of the pulses from a trace without noise and with noise without DPSS, respectively. We can see how the noise radically changes the spectrum of the pulse, and how the spectrum of a noisy pulse is modulated by the application of a DPSS on the pulse (in the time domain) (Figure 4-c). The panel (d), (e), and (f) show the logarithmic ratios, used in the SRM calculations. We can see how the ratios in Figure 4-f improve over the ones in Figure 4-e.

The results for the real data are shown in Figure 6. We laterally smoothed the retrieved Q-factor to correct for outliers estimations, and thus improve the visualization of the section.

Conclusions

In conclusion, this study has made significant contributions to the understanding and estimation of attenuation effects in seismic data analysis. The experiments conducted shed light on crucial considerations for accurate Q-factor estimation, including the definition of an appropriate frequency range and the use of advanced techniques such as DPSS tapering.

Our findings emphasize the importance of careful frequency selection to ensure reliable estimations within valid assumptions. Additionally, we observed that the utilization of previous peaks as a reference point yielded satisfactory results in noise-free synthetic scenarios, albeit with challenges in the presence of noise. To address these challenges and further improve our processing workflow, future work will incorporate the evaluation of the multi-window spectrum analysis method proposed by Freitas et al. (2023).

The incorporation of DPSS tapering demonstrated its effectiveness in enhancing Q-factor estimation compared to conventional methods. This approach effectively separated the desired seismic signal from background noise, leading to improved accuracy and robustness in Q-factor estimates.

While ongoing work is being conducted to estimate the Q-factor in real data from the Búzios oil field, in the Santos Basin, Brazil, the preliminary findings highlight the continuous efforts required for method refinement and the need for further studies. These include investigations into frequency recovery and the assignment of Q-values under varying conditions.

Acknowledgments

The authors gratefully acknowledge support from PETROBRAS (Petróleo Brasileiro S. A.) through the R&D "Seismic modeling data oriented to pre-salt reservoirs" (Agreement no. 5850.0107681.18) project at Fluminense Federal University (UFF) and the strategic importance of the support given by National Agency for Petroleum (ANP) through the RD levy regulation. Authors would like to thank the Seismic Imaging and Seismic Inversion Group (GISIS) team for all knowledge shared and also would like to thank UFF and Oceans and Land Dynamics graduate program (PPGDOT) for the all infraestructure to develop this work. Also the authors would like to Rodrigo S. Stern (UFF/GISIS) for the crucial TI support.

References

Freitas, D. F., M. Cetale, A. G. Figueiredo, L. A. Santos, and D. M. S. Filho, 2023, Multi-window spectrum analysis of búzios oil field PSDM seismic data applied to frequency attenuation study: Journal of Applied Geophysics, **213**, 105015.

Gamar-Sadat, F., P. Guillaume, A. Pica, G. Pignot, P. Poggi, A. Henry-Baudot, A. Prescott, A. Gacha, D. Carotti, and V. Prieux, 2015, Automatic gas pockets detection by high-resolution volumetric q-tomography using accurate frequency peak estimation: 77th EAGE Conference and Exhibition 2015, European Association of Geoscientists & Engineers, 1–5.

Kjartansson, E., 1979, Constant Q-wave propagation and attenuation.: Journal of Geophysical Research, **84**, 4737–4748.

Knopoff, L., and G. J. F. MacDonald, 1958, Attenuation of small amplitude stress waves in solids: Rev. Mod. Phys., **30**, no. 4, 1178–1192.

Kolsky, H., 1956, Lxxi. the propagation of stress pulses in viscoelastic solids: Philosophical magazine, **1**, 693–710.

———, 1964, STRESS WAVES IN SOLIDS: Journal of Sound Vib, 88–110.

Ramos, E. C., F. T. da Costa, M. A. C. Santos, L. A. Santos, et al., 2019, Frequency domain q analysis and stabilized inverse q filtering: Blake ridge data application.

Slepian, D., 1978, Prolate spheroidal wave functions, fourier analysis, and uncertainty — v: the discrete case: The Bell System Technical Journal, **57**, 1371–1430.

Wang, Y., 2008, Seismic inverse Q filtering: Wiley.

Zhang, C., and T. J. Ulrych, 2002, Estimation of quality factors from CMP records: Geophysics, **67**, 1542–1547.

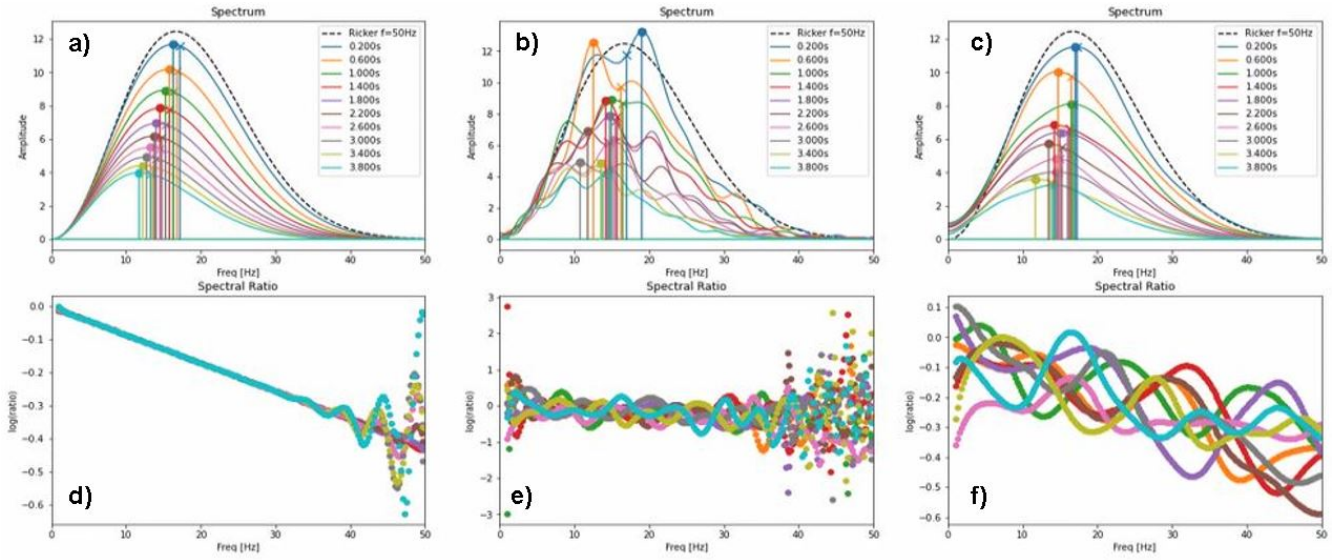

Figure 4: Spectrum of the pulses from trace (a) without noise, (b) with noise without any operation, (c) with noise and a 0^{th}-order DPSS ($NW = 3$) applied in each pulse; (d), (e), and (f) show their respective spectral logarithmic ratio (used in the SRM Q-factor estimation).

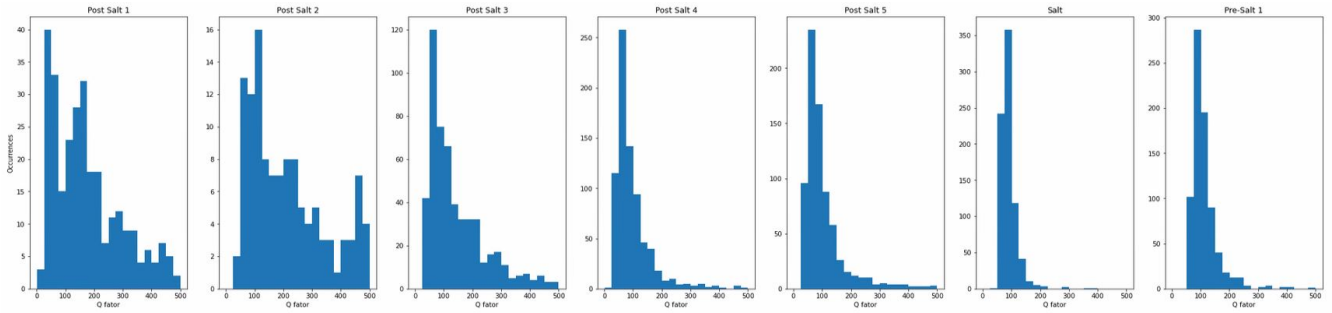

Figure 5: Q distribution for each layer.

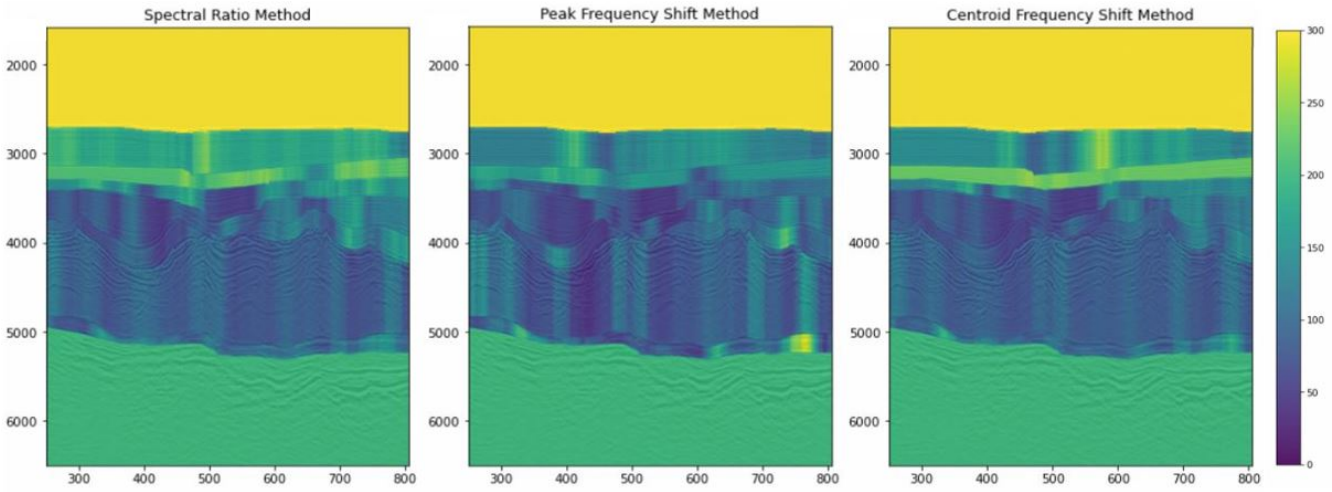

Figure 6: Q-factor sections from the same seismic line in the Santos basin using SRM (left), PFSM (center), and CFSM (right panel).